No-compromise 3D finite-element modeling of borehole DAS data

Andrey Bakulin[1], *Jacob Badger*[1,2], *and Sergey Fomel*[1], [1]*Bureau of Economic Geology, University of Texas at Austin,* [2]*FrequenSol, LLC*

Summary

We present a no-compromise modeling framework for borehole seismic applications, utilizing full-physics 3D finite-element simulations with adaptive meshing. This approach enables detailed and realistic modeling of complex wave phenomena in boreholes, including tube, body, and slow Krauklis waves in fluid-filled fractures. Our study employs a cross-well geometry inspired by upcoming hydrogen injection tests at the Devine Test Site to validate this capability across multiple physical interactions. By explicitly modeling the casing, completion, fluid coupling, perforations, and fiber configurations, we demonstrate how the complexity of the wavefield—particularly tube-to-Krauklis wave conversions and realistic DAS responses—is influenced by borehole construction and fluid coupling details. The numerical results exhibit strong sensitivity of wavefield attributes to hydraulic connectivity, fracture geometry, and DAS cable layout.

Introduction

The rapid proliferation of distributed fiber-optic sensing in recent years has enabled a broad range of geophysical applications, from surface seismic with surface-trenched DAS (Bakulin et al., 2020) to DAS VSP imaging using fiber cables in boreholes (Mateeva et al., 2017). Moreover, in boreholes, DAS is utilized across multiple spatial scales. At the largest scale, DAS supports seismic imaging from hundreds of meters to kilometers away from the well, facilitating vertical seismic profiling (VSP), 3D imaging, and time-lapse monitoring (Mateeva et al., 2017; Pevzner et al., 2021). At intermediate distances, DAS enables cross-well imaging over tens to a few hundred meters, providing high-resolution insights into the interwell zone (Beloborodov et al., 2024). Near the wellbore, DAS supports completion diagnostics—assessing perforation efficiency, screen integrity, and damage zones (Bakulin et al., 2008). Within the borehole itself, DAS can monitor dynamic multiphase flow behavior in real time, including gas–liquid interface movement throughout the entire well column (Ekechukwu et al., 2023).

Most DAS applications today center around fibers deployed in producing or injecting boreholes. Quantitative interpretation of all borehole measurements critically depends on correctly understanding and modeling fiber interaction with the borehole, completion, and fluid— especially for fiber-optic cables deployed on tubing, behind casing, or within the fluid. These details are poorly understood and often ignored, leading to a predominant reliance on traveltime information from borehole measurements with both geophones and DAS (Daley et al.,

2010; Beloborodov et al., 2024). Amplitudes are used only qualitatively for monitoring with permanent source-receiver placements (Zhu et al., 2015).

Likewise, surface-trenched fiber-optic cables exhibit even wider performance variations. Offshore conventional telecom cables deliver promising *P*-wave images (Raknes et al., 2023), whereas onshore straight DAS cables typically fail to produce any *P*-wave images. Even 30-degree helically wrapped fiber cables struggle to record upgoing *P*-wave reflections (Bakulin et al., 2022). This suggests that incorporating details of cable geometry and interactions with the surrounding solid is paramount for designing successful DAS sensing systems deployable from onshore to offshore. As a result, surface-based DAS remains a less mature area, with challenges in coupling and deployment limiting broader adoption despite promising early results (Bakulin et al., 2020).
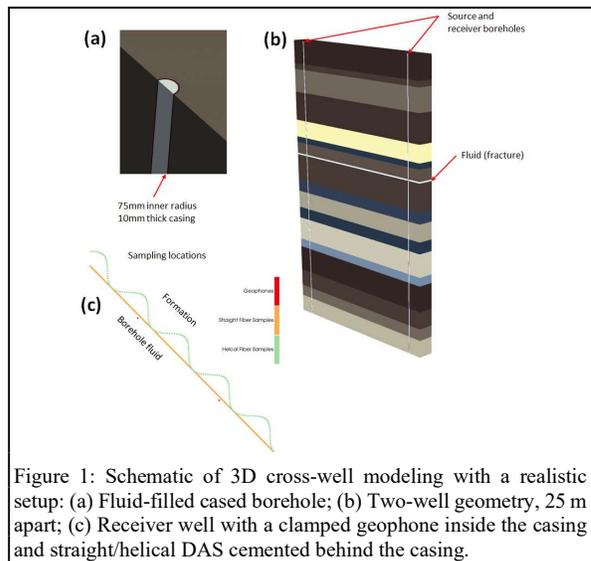

Figure 1: Schematic of 3D cross-well modeling with a realistic setup: (a) Fluid-filled cased borehole; (b) Two-well geometry, 25 m apart; (c) Receiver well with a clamped geophone inside the casing and straight/helical DAS cemented behind the casing.

In this study, we demonstrate how a numerical tool based on finite-element modeling (FEM) with adaptive mesh refinement can address key challenges in quantitative interpretation and enable rapid progress in the design of novel fiber-optic cables for seismic imaging. We achieve this by conducting a detailed 3D cross-well case study that incorporates realistic borehole elements—including well casing, fluid completion, and geophone and DAS placements both inside and outside the casing. The underlying algorithms, including a scalable multigrid solver

for viscoelastic frequency-domain simulations, have been documented elsewhere (Badger, 2024a,b); therefore, we do not revisit algorithmic details here. Instead, we use this case study to selectively highlight FEM capabilities most critical for accurately simulating complex borehole wave phenomena.

Cross-well modeling with boreholes and DAS
Let us demonstrate the capabilities using a cross-well seismic survey shown in Figures 1 and 3. The model and survey geometry are inspired by the hydrogen injection test planned at the Devine Test Site (Bakulin et al., 2024). We emphasize that the modeling is fully 3D, so no compromises are made in simulating the full complexity of wave propagation, including tube waves in the borehole and their conversion to and from body waves—phenomena that are pronounced in borehole surveys (Bauer et al., 2005; Ziatdinov et al., 2006b; Watanabe et al., 2004).

We further enhance geological realism by introducing a 25-cm open, fluid-filled fracture intersecting both boreholes—enabling the simulation of the slow Krauklis wave (Krauklis, 1962; Goloshubin et al., 2012). This guided mode is highly sensitive to fracture geometry and fluid properties, making it a valuable diagnostic for characterizing hydraulic fracture intersecting the boreholes (Derov et al., 2009; Liang et al., 2017; Ziatdinov et al., 2006a).
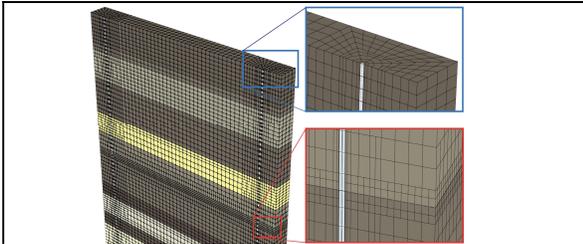

Figure 2: Adaptive meshing shown around the source borehole.

Previous studies have attempted to couple low-frequency wave propagation in boreholes and layered media with fluid-filled fractures using semi-analytical or approximate modeling techniques to explore tube-to-slow wave conversions and vice versa. However, these methods were difficult to validate and inherently limited—they could not capture the full complexity of borehole completions, including casing, cement, fluid layers, or perforations—leaving interpretation largely qualitative at best (Derov et al., 2009; Liang et al., 2017; Ziatdinov et al., 2006a).

To support such detailed modeling, the FEM solver must resolve fine-scale geometric features like casing, fluid layers, and perforations while maintaining computational efficiency across the entire 3D domain. This is achieved through adaptive meshing, which concentrates grid resolution where it is most needed—around boreholes and fractures—while coarsening elsewhere to reduce cost.

Figure 2 illustrates this adaptive meshing strategy, demonstrating how a relatively simple mesh with curvilinear hexahedral elements can accurately capture the complex borehole geometry, including concentric layering and sharp material interfaces.

Simulations are performed in the frequency domain across a range of frequencies, which are then combined to reconstruct the time-domain response. Frequency-domain (FD) snapshots are an effective tool for initial quality control (Figure 3). For example, at 2000 Hz, a snapshot from a sparker source placed in the fluid-filled cased borehole reveals key features of the wavefield and energy distribution. Most energy is confined to tube waves traveling along the borehole, which convert into slow Krauklis waves within the fluid-filled fracture and guided modes in the underlying low-velocity layer. In the receiver well, both components further convert into upgoing tube waves. In contrast, body waves traveling through the formation are much weaker. Additional tube-to-body conversions occur at borehole interfaces, particularly where material contrasts exist, resulting in weaker arrivals across the interwell space.

Analysis of the wavefield with and without boreholes
Let us now demonstrate the essential role of modeling borehole complexity in cross-well surveys in more detail. Ignoring borehole effects—treating the source and receiver as if they were embedded directly in the subsurface—results in the gathers shown in Figure 4. With a volumetric source (200–550 Hz), we observe expected omnidirectional radiation, with most of the energy propagating as direct body P-waves. These are strongest on the X-component along the horizontal wavepath (Figur 4b). Shear waves are not directly excited by a volumetric source.

In contrast, the presence of boreholes produces a much more complex energy distribution and radiation pattern, as shown in Figure 5. A sparker source inside fluid-filled, steel-cased boreholes generates a far-field pattern containing both P- and S-wave components (Gibson et al., 2005). This radiation can be interpreted as a superposition of a volumetric source and a vertical dipole (Ben-Menahem and Kostek, 1991). Since much of the energy is trapped in the borehole as tube waves, the body P-wave arrival becomes significantly weaker (Figure 5b), while the direct S-wave dominates. A zoom into Figure 8a confirms that the S-wave radiation pattern exhibits the characteristic polarity reversal of a vertical dipole along the horizontal propagation direction.

Without boreholes, the direct body P-wave from the source couples weakly into a slow Krauklis wave (Derov et al., 2009), as observed on the horizontal component in the receiver well (Figure 4b). In contrast, the presence of boreholes leads to stronger tube waves propagating along the source borehole and converting more efficiently into a

prominent Krauklis wave traveling along the fluid-filled fracture (Figure 5b).
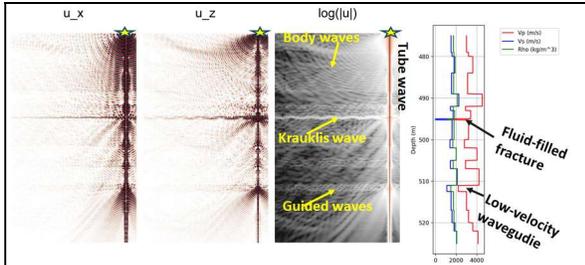

Figure 3. Frequency-domain snapshot at 2000 Hz (sparker source in borehole) showing wavefield energy balance. Energetic tube waves propagate along the borehole and convert into Krauklis waves in the fracture and guided modes in the low-velocity layer. Weaker body waves and tube-to-body conversions also appear, along with lower-energy tube waves in the receiver well.

Similarly, the Krauklis wave couples back effectively into the tube wave in the receiver borehole, visible on the vertical component (Figure 5a). Tube waves often carry significant surveillance information in cross-well and in-well monitoring (Korneev et al., 2006; Watanabe et al., 2005; Bauer et al., 2005; Ziatdinov et al., 2006a,b). However, quantitative modeling of tube wave interactions with borehole completions, layering, and fluid interfaces remains challenging. As a result, many monitoring techniques remain qualitative, even though detailed completion designs are typically well known.

Likewise, Krauklis waves guided by hydraulic fractures are a critical diagnostic tool for fracture characterization (Derov et al., 2009; Liang et al., 2017). However, their complex physics remains challenging to model quantitatively, which impedes the development of robust inversion approaches for resolving detailed fracture geometry and connectivity.

Hydraulic communication between the borehole and the fracture is a key factor controlling the efficiency of tube-to-Krauklis wave conversion. Previous studies have explored this interaction using semi-analytical and numerical approaches with simplified completion geometries (Ziatdinov et al., 2006a; Bakulin et al., 2005). Figure 6 illustrates the impact of fluid connectivity by comparing cases with unperforated and perforated casing, where the latter is modeled as a casing break across the fluid-filled fracture. Frequency-domain snapshots reveal a markedly stronger Krauklis wave in the perforated case (Figure 6b), confirming the well-established role of hydraulic connection in enhancing energy transfer into fracture-guided modes. These FD simulations provide efficient and accurate estimates of frequency-dependent conversion coefficients, which are otherwise only available through analytical approximations for idealized, axisymmetric settings (Bakulin et al., 2006). Meanwhile, finite-element modeling (FEM) enables the incorporation of realistic completion

details—such as discrete perforations—that critically influence wavefield behavior and conversion efficiency.
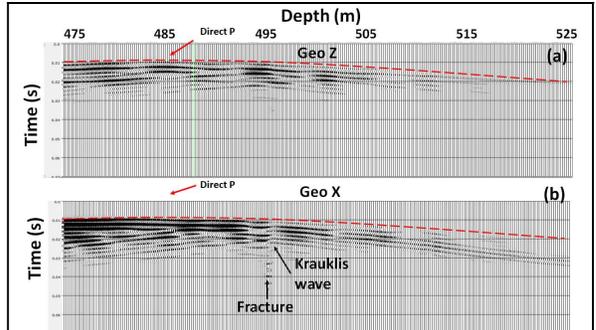

Figure 4. Geophone wavefield in the receiver well from cross-well simulations (Figures 1 and 2) with a volumetric source: (a) Z-component, (b) X-component. Boreholes are not explicitly modeled—sensors are embedded directly in the formation.
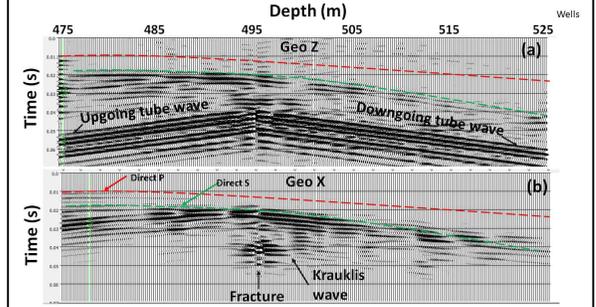

Figure 5. Same as Figure 4, but with boreholes modeled. The sparker source is centered in the fluid-filled cased borehole (Figure 1a), and geophones are clamped inside the casing (Figure 1c).

Measuring Krauklis wave dispersion on FD snapshots
Frequency-domain snapshots are also helpful for directly evaluating the dispersion of slow interfacial waves, such as Krauklis waves, in fluid-filled fractures. Figure 7 provides an example using snapshots at two frequencies for a more realistic 10 mm fracture. By estimating the spatial wavelength at each frequency, we compute the phase velocity—approximately 280 m/s at 100 Hz (Figure 7a) and 580 m/s at 1000 Hz (Figure 7b) - demonstrating the strong dispersive nature of the Krauklis wave. While dispersion for planar fractures can be calculated analytically (Krauklis, 1962; Liang et al., 2017), finite-element modeling enables numerical evaluation in more realistic settings, such as rough-walled fractures containing proppant or other heterogeneities.

Simulating the realistic DAS response
Finally, we demonstrate that numerical simulations can also predict realistic responses recorded by DAS cables in various configurations using a methodology similar to Egorov et al. (2021). Figure 8 compares wavefields recorded above the fluid-filled fracture by three sensing types: vertical

geophones clamped to the casing, straight DAS cemented behind the casing, and helical DAS behind the casing.
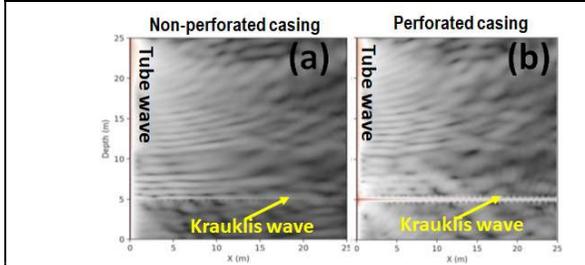

Figure 6. Modeling tube-to-Krauklis wave conversion shows stronger conversion for perforated (b) compared to unperforated (a) casing, due to improved fluid communication. The simulation assumes a 10 mm fracture and 1000 Hz source.
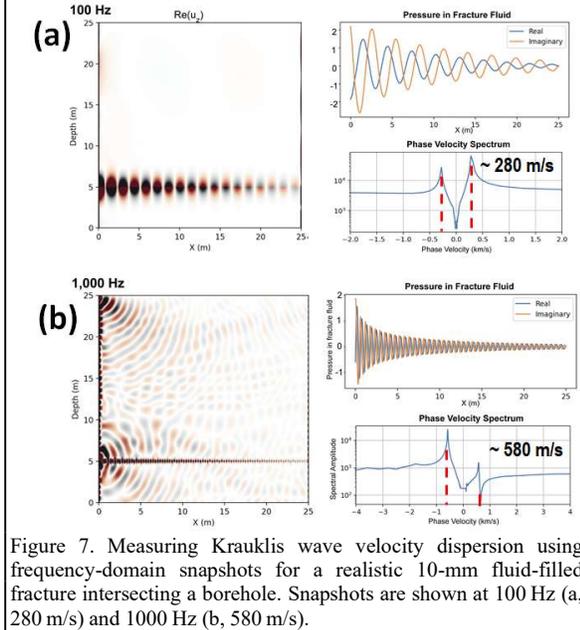

Figure 7. Measuring Krauklis wave velocity dispersion using frequency-domain snapshots for a realistic 10-mm fluid-filled fracture intersecting a borehole. Snapshots are shown at 100 Hz (a, 280 m/s) and 1000 Hz (b, 580 m/s).

The DAS response clearly differs from the geophone data. The straight DAS, which behaves most similarly to the vertical geophone, captures minimal P-waves but effectively records S-waves. Unlike the geophone, the straight DAS does not exhibit polarity reversal along the horizontal propagation direction (Figure 8a vs. 7c); instead, it shows *S*-wave polarity reversal at an oblique angle (indicated by the blue arrow in Figure 8c), a feature not observed in the geophone data.

In contrast, the helical DAS acts more like a horizontal geophone, prominently capturing direct *P*-waves. However, it shows a slightly altered amplitude radiation pattern with noticeable dimming (Figure 8d), likely due to spatial averaging introduced by the 2-meter gauge length. Unlike

the straight DAS, the helical configuration does not show polarity reversal but instead emphasizes *P*-wave energy, consistent with its directional sensitivity.

These simulations confirm that DAS directionality and gauge-length averaging significantly affect recorded wavefields and must be accurately modeled for effective survey design and quantitative interpretation of DAS borehole data.
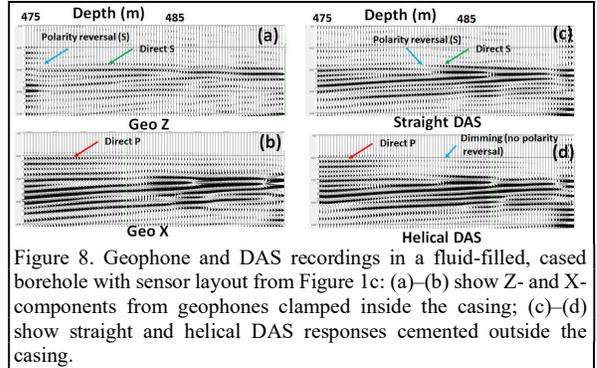

Figure 8. Geophone and DAS recordings in a fluid-filled, cased borehole with sensor layout from Figure 1c: (a)–(b) show Z- and X-components from geophones clamped inside the casing; (c)–(d) show straight and helical DAS responses cemented outside the casing.

Conclusions

In this study, we have demonstrated the capability of finite-element viscoelastic modeling with adaptive meshing to effectively handle complex wave propagation, including borehole tube waves and DAS responses. We used well-studied examples from cross-well seismic surveys with high-frequency sources between two fluid-filled, steel-cased boreholes to perform this demonstration. Complete, no-compromise 3D physics enables accurate modeling of the exact energy distribution between body and tube waves, as well as an evaluation of the conversion of tube waves into slow Krauklis waves within fluid-filled fractures.

Using known examples, we demonstrate that the finite-element method accurately replicates established physics derived from analytical and semi-analytical solutions. This validation sets the stage for uncompromised modeling of more complex scenarios involving realistic completions, including casing, tubing, perforations, and fluid-filled fractures with asperities and rough surfaces.

We highlight the importance of simulating DAS responses, which significantly differ from clamped geophones. Incorporating all wave events, including P-waves, S-waves, tube waves, and Krauklis waves and their interactions, provides a comprehensive toolset for successful borehole monitoring in cross-well and in-well scenarios. The proposed framework supports next-generation borehole monitoring designs and enables robust inversion workflows grounded in full-physics understanding.

No-compromise 3D borehole modeling of DAS

References

Badger, J., 2024a, Scalable DPG Multigrid Solver with Applications in High-Frequency Wave Propagation: PhD Thesis, University of Texas at Austin.

Badger, J., Bakulin A., and S. Fomel, 2024b, Scalable, efficient, and adaptive simulation of frequency-domain wave propagation, SEG Technical Program Expanded Abstracts, 1796-1800. https://doi.org/10.1190/image2024-4101625.1

Bakulin, A., Shuster, M., Bhattacharya, S., Delshad, M., Alhotan, M., Li, C. and Rohatgi, A., Field-Test Design for Geophysical Monitoring of Hydrogen Injection in Water-Bearing Layer, 2024 Fall Meeting, American Geophysical Union, Abstract MR13A-3177, Washington, DC.https://doi.org/10.22541/essoar.173627314.46466893/v1

Bakulin, A., Alfataierge, E., Pevzner, R., and K. Tertyshnikov, 2022, Evaluating HD weathering surveys and surface seismic with DAS in a sand dune environment, SEG Technical Program Expanded Abstracts, 621-625.

Bakulin, A., Silvestrov, I., and R. Pevzner, 2020, Surface seismic with DAS: an emerging alternative to modern point-sensor acquisitions: The Leading Edge, 39, 808-818

Bakulin, A., Sidorov, A., Kashtan, B., Jaaskelainen, M., 2008, Real-time completion monitoring with acoustic waves: Geophysics, 73, E15-E33

Bakulin, A., Gurevich, B., Ciz, R. and S. Ziatdinov, 2005, Tube-wave reflection from a porous permeable layer with an idealized perforation, SEG Technical Program Expanded Abstracts, 332-335. https://doi.org/10.1190/1.2144335

Bauer, K., R.G. Pratt, M. H. Weber, T. Ryberg, C. Haberland, and S. Shimizu, 2005, The Mallik 2002 crosswell seismic experiment: Project design, data acquisition and modeling studies; in Scientific Results from the Mallik 2002 Gas Hydrate Production Research Well Program, Mackenzie Delta, Northwest Territories, Canada, (ed.) S. R. Dallimore, and T. S. Collett: Geological Survey of Canada, Bulletin 585.

Beloborodov, N., Tertyshnikov, K., Collet, O., Isaenkov, R., Vorobev, M., Shashkin, P., Gurevich, B., and Pevzner, R. 2024, A field trial of cross-well seismic with DAS and a high-frequency source. 1st ASEG DISCOVER Symposium 2024, October 15-18, Hobart, Australia.

Ben-Menahem, A. and S. Kostek, 1991, The equivalent force system of a monopole source in a fluid-filled open borehole, GEOPHYSICS 56: 1477-1481. https://doi.org/10.1190/1.1443168

Daley, T.M., Niu, F., Silver, P.G., Majer, E.L., 2010, Acquisition of Crosswell Seismic Monitoring Data: Handbook of Geophysical Exploration: Seismic Exploration, 40, 165-176. https://doi.org/10.1016/S0950-1401(10)04014-0

Derov, A., Maximov, M., Lazarkov, M., Kashtan, B., and A. Bakulin, 2009, Characterizing hydraulic fractures using slow waves in the fracture and tube waves in the borehole: 79th Annual International Meeting, SEG, Expanded Abstracts, 4115-4119

Devine Test Site, BEG UT Austin: https://www.beg.utexas.edu/about/facilities/dts/devine-test-site, accessed January 14, 2025.

Anton Egorov, Marwan Charara, Ezzedeen Alfataierge, and Andrey Bakulin, 2021, Realistic modeling of surface seismic and VSP using DAS with straight and shaped fibers of variable gauge length, SEG Technical Program Expanded Abstracts, 437-441. https://doi.org/10.1190/segam2021-3576626.1

Ekechukwu, G. K., Sharma, J., and M. J. William, 2023, A novel velocity band energy workflow for fiber-optic DAS interpretation and multiphase flow characterization: Scientific Reports, 13, 15142. https://doi.org/10.1038/s41598-023-42211-0

Gibson, R. L., Turpening, W. R., Born, A., & Turpening, R. M., 2005, Seismic sources in cased and cemented boreholes. SEG Technical Program Expanded Abstracts, 313-316. https://doi.org/10.1190/1.1822468

Goloshubin, G., Korneev, V., Kashtan, B., Bakulin, A., Troyan, V., Maximov, G., Molotkov, L., Frehner, M., Shapiro, S., Shigapov, R., 2012, Krauklis Wave - Half a Century After: 5th EAGE St.Petersburg International Conference and Exhibition on Geosciences - Making the Most of the Earths Resources, cp-283-00051. https://doi.org/10.3997/2214-4609.20143641

Korneev, V., Bakulin, A., and S. Ziatdinov, 2006, Tube-wave monitoring of oil fields, SEG Technical Program Expanded Abstracts, 374-378. https://doi.org/10.1190/1.2370279

Krauklis, P. V., 1962, About some low frequency oscillations of a liquid layer in elastic medium: Prikladnaya Matematika i Mekhanika, 26, 1111–1115, in Russian.

Liang, C., O'Reilly, O., Dunham, E. and D. Moos, 2017, Hydraulic fracture diagnostics from Krauklis-wave resonance and tube-wave reflections, GEOPHYSICS 82: D171-D186.
https://doi.org/10.1190/geo2016-0480.1

Mateeva, A., Lopez, J., Potters, H., Mestayer, J., Cox, B., Kiyashchenko, D., Wills, P., Grandi, S., Hornman, K., Kuvshinov, B., Berlang, W., Yang, Z., Detomo, R., 2014, Distributed Acoustic Sensing for Reservoir Monitoring with Vertical Seismic Profiling: Geophysical Prospecting, 62(4), 679-692. https://doi.org/10.1111/1365-2478.12116

Pevzner, R., Isaenkov, R., Yavuz, S., Yurikov, A., Tertyshnikov, K., Shashkin, P., Gurevich, B., Correa, J., Glubokovskikh, S., Wood, T., Freifeld, B., Barraclough, P., 2021. Seismic monitoring of a small CO2 injection using a multi-well DAS array: Operations and initial results of Stage 3 of the CO2CRC Otway project. International Journal of Greenhouse Gas Control, 110, 103437. https://doi.org/10.1016/j.ijggc.2021.103437

Raknes, E.B., Ivanov, Y., Eikrem, K.S., Bertrand, A., Buizard, S., Poletto, F., 2023, Seabed distributed acoustic sensing (SB-DAS) imaging in the North Sea: A case study using existing telecommunication cables: First Break, 41(3), 57-62. https://doi.org/10.3997/1365-2397.fb2023019

Watanabe, T., S. Shimizu, E. Asakawa, and T. Matsuoka, 2004, Differential waveform tomography for time-lapse crosswell seismic data with application to gas hydrate production monitoring: 74th Annual International Meeting, SEG, Expanded Abstracts, 2323–2326.

Zhu, T., Ajo-Franklin, J.B., Daley, T.M., 2015, Spatiotemporal changes of seismic attenuation caused by injected CO2 at the Frio-II pilot site, Dayton, TX, USA: Geophysical Research Letters, 42(21), 9249-9257. https://doi.org/10.1002/2015GL066069

Ziatdinov, S., Bakulin, A, and B. Kashtan, 2006a, Tube-Wave Interaction with a Fluid-Filled Circular Fracture of a Finite Radius: 68th EAGE Conference and Exhibition incorporating SPE EUROPEC 2006, Expanded Abstracts, P023.

Ziatdinov, S., Bakulin, A, Kashtan, B., Korneev, V., and A. Sidorov, 2006b, Tube-wave monitoring at Mallik field: comparing modeled and experimental time-lapse responses: 76th Annual International Meeting, SEG, Expanded Abstracts, 3240-4244.